

Determining the profile of textured membranes by the alpha particle energy loss method

C. Kaiser,^{a)} Y. Levy, T. Tiedje, and Jeff F. Young

Department of Physics and Astronomy, University of British Columbia, Vancouver, B.C. Canada, V6T 1Z1

I. Kelson

School of Physics and Astronomy, The Raymond and Beverly Sackler Faculty of Exact Sciences, Tel Aviv University, Tel Aviv 69978, Israel

(Received 11 September 2001; accepted for publication 7 February 2002)

Alpha particle energy loss (AEL) spectroscopy was used to characterize a 5 μm pitch grating of silicon bars on a silicon dioxide membrane. Comparison of the data with simulated spectra shows that the angle of nonvertical grating sidewalls are readily quantified by AEL. The potential of AEL for distinguishing undercut and overcut etch profiles is assessed. © 2002 American Institute of Physics. [DOI: 10.1063/1.1468268]

The alpha particle energy loss (AEL) method has been used in recent years as a diagnostic tool in the growth and processing of semiconductor thin films. The method consists of implanting alpha emitters in the substrate of films to be processed and measuring the energy lost by the alpha particles that pass through the film. Applications include online growth rate monitoring¹ and stoichiometric analysis of thin films grown by molecular-beam epitaxy,² and geometric mapping of nonplanar surfaces.³ AEL has also been applied as an *in situ* monitor of plasma etching for the determination of etch rates, endpoints, and depths of one-dimensional (1D) gratings etched through masks.⁴

In this letter, we describe an application of the AEL method to the characterization of periodic gratings on free-standing membranes. Free-standing semiconductor membranes textured with deep-etched submicron hole patterns represent a class of two-dimensional photonic crystals⁵⁻⁷ that have already been used as a host for microcavity lasers.⁸ The sidewall angle of the holes etched into these membranes can be quite important, but it is very difficult to nondestructively measure their profile. Next, we show how the AEL technique can be used as a nondestructive means of determining the membrane thickness, the grating depth and duty cycle, and the angle of the grating sidewalls. This is all demonstrated using 1D gratings etched into an 800 nm thick silicon layer supported on a 1 μm thick silicon dioxide membrane. We begin with a brief summary of the relevant features of the AEL method. We then describe the membrane fabrication process and the simple simulation used to fit the observed alpha spectra. The results and conclusions are presented last.

Profiling the thickness of a thin film is effected, in principle, by allowing a parallel, spatially uniform beam of monoenergetic alpha particles to go through it. If we assume, for simplicity, that the amount of energy lost by an alpha particle is exactly proportional to the length of its trajectory in the film material, then each surface element will give rise to an alpha energy according to its thickness, resulting in a well defined alpha-energy spectrum. By parameterizing the sur-

face profile in simulations of the alpha-particle trajectories, it is possible to deduce the shape of the etched surface from the observed spectra. To illustrate our basic methodology, we show in Fig. 1 a schematic representation of a membrane grating of period A , where all the segments are assumed to be straight lines. There are altogether four independent parameters which characterize the periodic cross section, as defined in the caption of Fig. 1. The alpha spectrum corresponding to our idealization of the grating and the alpha-source beam is shown in Fig. 2 where two sharp peaks are joined by a continuum of counts stretched between them. The energy shift of the upper peak relative to the original alpha energy is proportional to h_1 . The energy difference between the two peaks is proportional to h_2 . The fraction of counts in the higher peak, in the lower peak, and in the intermediate region are equal to $(A - b_1)/A$, b_2/A and $(b_1 - b_2)/A$, respectively.

In reality a number of factors complicate this simple picture. For example, the real alpha source is not collimated. Rather, a collimating plate in front of the detector is used to restrict the angular range over which particles may be detected. A dispersion of path lengths arises over this range. Also, though the trajectories are virtually straight, the energy loss is not simply proportional to the amount of material traversed: account must be taken of the nonlinear dependence of the energy loss rate on the energy itself, and on statistical straggling effects. Finally, for any given energy loss, the actual recorded value will be modified by the intrinsic resolution of the detector (about 35 keV in our case). All of these complicating effects are easily taken account of in a simple simulation model, which was used to perform least-squares fits to the observed spectra. The simulation we have

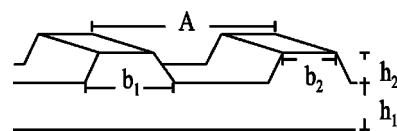


FIG. 1. Idealized profile of a 1D grating structure with period A . The parameters that characterize the profile are the thickness of the grating base, h_1 , the height of the ridge, h_2 , and the width of the ridge at its bottom and at its top, b_1 and b_2 , respectively.

^{a)}Electronic mail: ckaiser@physics.ubc.ca

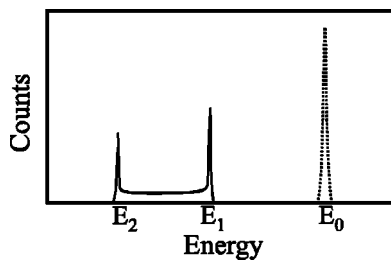


FIG. 2. (dotted line): Idealized alpha-source energy spectrum centered at the original alpha energy E_0 ; (solid line): Idealized alpha particle energy spectrum corresponding to the 1D membrane grating structure shown in Fig. 1. The peaks centered at energies E_1 and E_2 are due to particles passing through the grating trough and ridge, respectively. Particles that pass through the grating sidewalls contribute to counts in the interpeak region.

constructed accounts for dispersion due to the finite angular range of incidence by first selecting a discrete set of incident angles that are representative of the total angular range. Then, for each incident angle in the set, the associated spectrum is calculated. The simulated spectrum is constructed as the sum over the discrete set of the associated spectra. Dispersion due to straggling has a Gaussian distribution, as does the finite resolution of the detector, though the former increases in proportion to the energy loss, whereas the latter is constant. The variance due to each source of dispersion determines the variance of the Gaussian distribution with which the simulated spectrum is convolved.

The membrane structure was fabricated from a silicon-on-insulator (SOI) wafer consisting of a 1 μm thick oxide sandwiched between layers of $\langle 100 \rangle$ float zone silicon. Above the oxide was a 1 μm silicon thin film that formed the polished surface of the wafer. Beneath the oxide was 550 μm of bulk silicon. Ultimately, the bulk silicon was fashioned into a support structure for the thin films that were left free standing in 3 mm^2 rectangular regions where the bulk silicon was removed. The silicon thin film was formed into a 5 μm pitch, 1D grating. The oxide thin film remained as the uniform base of the membrane structure. The fabrication process began with the growth of a thermal oxide, 420 nm thick, on both surfaces of the SOI wafer. Subsequent processing was performed on 1 cm^2 samples that were cleaved from the oxidized wafer. The oxide on the thin-film side of the wafer was masked with a 5 μm pitch grating of photoresist. Buffered HF was used to transfer the grating pattern from the resist to the oxide, to a depth of 100 nm. Next, both oxide surfaces were masked uniformly in photoresist. The resist on the bulk side was removed in rectangular regions that measured 1.5 $\text{mm} \times 5$ mm. The exposed slots of oxide were then stripped in buffered HF, thus exposing the silicon bulk. A silicon etchant, ethyldiamine pyrocatechol, EDP, heated to 90°C, was used to remove the bulk silicon from the slotted regions. EDP etches the $\langle 100 \rangle$ plane of silicon at more than 15 times the rate at which it etches the $\langle 111 \rangle$ plane. The $\langle 111 \rangle$ planes, which define the walls of the etched regions, stand at 35.26° off the vertical. Each 1.5 $\text{mm} \times 5$ mm slot etched in the silicon bulk sloped inward from its base and defined a slot measuring approximately 0.7 $\text{mm} \times 4.2$ mm at the thin-film side of the sample, where the 1 μm oxide of the original SOI structure was exposed. The sample was next immersed in the buffered oxide etchant until the thin regions of the thermal oxide grating were completely removed and its

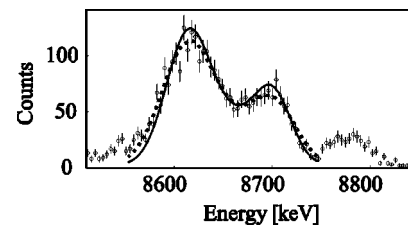


FIG. 3. AEL spectrum (discrete points) for the membrane structure of Fig. 4 with best fit simulation with a broadening function of 35 keV (solid line) and 45 keV (dotted line).

thickness in the ridge regions was between 50 and 100 nm. Finally, the grating pattern of oxide strips was transferred to the silicon thin film by a 1 min immersion of the sample in the hot EDP.

The alpha source utilized to image the membrane structure was prepared by implanting in an auxiliary silicon substrate about 0.3 microcuries of ^{224}Ra (3.7 days half life) by exposure of the polished surface of the substrate to a planar source of ^{228}Th (1.9 years half life). Ultimately, the implanted substrate contains all the isotopes in the $^{224}\text{Ra} \rightarrow ^{208}\text{Pb}$ decay chain⁹ with a multiplicity of distinct primary alpha energies—5.69, 6.05, 6.28, 6.79, and 8.78 MeV. We have chosen, for the purpose of this presentation, to limit the analysis to the highest energy alpha particle, which gives the purest spectrum. A collimator, perpendicular to the surface, defined an angular acceptance of $\pm 5^\circ$.

The experimentally observed alpha spectrum is shown in Fig. 3 along with the simulated spectra for each of two scenarios. In both scenarios, the fitting of the simulated spectrum to the observed one is carried out over a “region of interest” extending roughly from 8580 to 8750 keV. The experimental spectrum contains counts outside this region as well: about 9% of the total in a somewhat broadened peak at the original alpha energy; about 5% of the total distributed over lower energies corresponding to larger thicknesses. Upon inspection of the membrane, a number of cracks were discovered where the edge of the membrane curled onto itself, thus fully explaining the observations and justifying the use of a “region of interest”.

In Fig. 3, the solid line is the best fit line of the simulation for which the broadening function is constrained by the known width of the detector resolution (35 keV). The extracted geometric dimensions of this best fit line are shown to scale in Fig. 4, superimposed on an actual cross sectional view of the grating. The grating parameters extracted for this scenario are $b_1 = 4095 \pm 50$ nm, $b_2 = 2385 \pm 50$ nm, $h_1 = 825 \pm 20$ nm, and $h_2 = 885 \pm 30$ nm. This value for h_2 includes the 50 nm thick oxide mask that caps the ridges and overhangs the grating sidewalls, as can be seen in Fig. 4. The

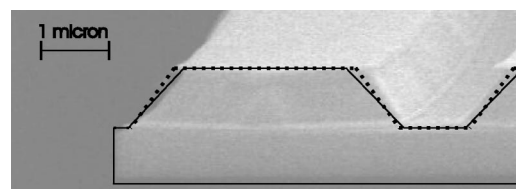


FIG. 4. Cross sectional view of the membrane grating overlaid with a sketch of the simulation profile that best fit the spectral data with a broadening function of 35 keV (solid line) and 45 keV (dotted line).

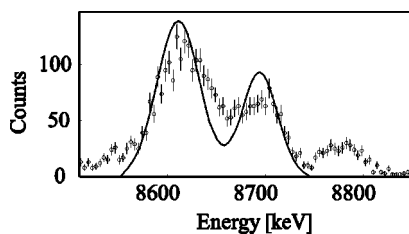


FIG. 5. AEL spectrum as in Fig. 3 with best fit simulation found under the constraint that the grating sidewalls were perfectly vertical.

average slope of the sidewalls, as determined by the simulation, is $44 \pm 4^\circ$. A slope value of $37 \pm 3^\circ$ was measured from scanning electron microscope images and a slope value of $< 38^\circ$ was derived by calculation from the preferential etch rates discussed herein. The relative largeness of the AEL slope value can be attributed to sources of broadening not accounted for in the simulation. For example, we did not account for broadening due to thickness variations in the etched regions of the membrane structure. If the broadening function in the simulation is not constrained by the detector resolution, we achieve the best fit line and extracted geometric profile of the dotted lines in Figs. 3 and 4, respectively, corresponding to a sidewall slope of $36 \pm 4^\circ$, for a broadening function of 45 keV. Figure 5 shows the best fit that can be obtained if the sidewalls are forced to be perpendicular to the membrane.

When the typical feature height of the etched sample (in our case the height of the ridge, h_2) is much greater than the height resolution of the detector ensemble, then it should be possible to use the AEL spectra for discriminating undercut or overcut etch sidewalls from sidewalls that slope linearly. A schematic demonstration of this ability is shown in Fig. 6. Three hypothetical sidewalls are drawn—one concave, one straight, and one convex—with the three corresponding alpha spectra that would result from their imaging. Finally, we note that by narrowing the acceptance angle of the detector collimator and then obtaining spectra at a range of mean trajectory angles, the overall accuracy and versatility of the method should be further enhanced.

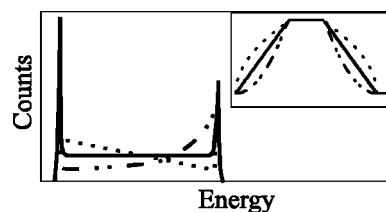


FIG. 6. Schematic energy spectra of undercut, linear and overcut etch sidewalls as shown in the inset.

In summary, we have demonstrated that it is possible to nondestructively determine the height, pitch, and sidewall profile of 1D gratings etched into thin semiconductor membrane structures using alpha-particle energy loss spectroscopy.

This work was supported by the Israeli Ministry of Science, Culture and Sport and by the Natural Sciences and Engineering Research Council in Canada. The authors give special thanks to D. Axen whose Monte Carlo simulations helped establish the validity of their simple model.

¹M. Beaudoin, Z. Gelbart, U. Giesen, I. Kelson, Y. Levy, J. A. MacKenzie, T. Pinnington, S. Ritchie, A. J. SpringThorpe, R. Streater, and T. Tiedje, *Surf. Coat. Technol.* **94**, 374 (1997).

²I. Kelson, Y. Levy, D. Racah, E. Redmard, M. Beaudoin, T. Pinnington, T. Tiedje, and U. Giesen, *J. Phys. D* **30**, 131 (1997).

³I. Kelson, C. V. Kaiser, Y. Levy, G. Biasiol, and E. Kapon, *Nucl. Instrum. Methods Phys. Res. B* **170**, 483 (2000).

⁴Y. Levy, A. Ballestad, M. Davies, Y. Feng, I. Kelson, W. J. Mandeville, V. Pacradouni, A. Schmalz, T. Tiedje, and J. F. Young, *Mater. Res. Soc. Symp. Proc.* **569**, 29 (1999).

⁵M. Kanskar, P. Paddon, V. Pacradouni, R. Morin, A. Busch, Jeff F. Young, S. R. Johnson, Jim MacKenzie, and T. Tiedje, *Appl. Phys. Lett.* **70**, 1438 (1997).

⁶S. G. Johnson, S. Fan, P. R. Villeneuve, and J. D. Joannopoulos, *Phys. Rev. B* **60**, 5751 (1999).

⁷M. Lončar, T. Doll, J. Vučković, and A. Scherer, *J. Lightwave Technol.* **LT18**, 1402 (2000).

⁸O. J. Painter, A. Husain, A. Scherer, J. D. O'Brien, I. Kim, and P. D. Dapkus, *J. Lightwave Technol.* **LT17**, 2082 (1999).

⁹C. M. Lederer and V. S. Shirley, *Table of Isotopes*, 7th ed. (Wiley, New York, 1977).